In Silico Blood Pressure Models Comparison

Ana Carolina Gonçalves Seabra, Alexandre Ferreira da Silva, Thomas Stieglitz, *Fellow, IEEE*, and Ana Belén Amado-Rey

***Abstract*—As cardiovascular diseases (CVDs) are one of the most prominent illnesses, continuous, noninvasive, and comfortable monitoring of blood pressure (BP) is indispensable. This article investigates the best method for obtaining highly accurate BP values in noninvasive measurements through the extraction of hemodynamic variables from the arteries of young subjects. After the literature review, five state-of-the-art BP models were analyzed and qualitatively compared in a novel in silico study. Relevant arterial parameters such as luminal area, flow velocity, and pulse wave velocity (PWV) of 1458 subjects were extracted from a computer-simulated database and served as input parameters in the BP models' simulation. The five models were calibrated to each arterial site. Contrary to the expected, the linear model (linear transformation of the distending diameter into BP) revealed more accuracy than the commonly used exponential transformation. In an ex vivo experimental setup, the linear model was used for the extraction of BP by using an ultrasound (US) sensor and validated with a commercial pressure sensor. The results showed an in silico pulse pressure (PP) correlation of 0.978 and a mean difference of (−2.845 ± 2.565) mmHg at the radial artery and an ex vivo PP correlation of 0.986 and a mean difference of (1.724 ± 3.291) mmHg. Thus, with the linear model, the US measurement complies with the Association for the Advancement of Medical Instrumentation (AAMI) standard with smaller deviations than ±5 mmHg.**

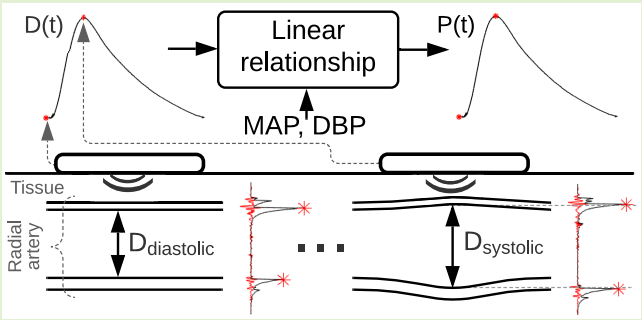

***Index Terms*—Arterial pressure waveform, continuous and noninvasive blood pressure (BP) measurement, hypertension monitoring, mathematical BP model, pulse pressure (PP), ultrasound (US) sensor.**

I. Introduction

HYPERTENSION is the most common cause of cardiovascular diseases (CVDs) worldwide. The higher the blood pressure (BP), the higher the risk of damage to the heart and blood vessels in the major organs. Hypertension is known as the "silent killer," causing around half of all deaths from CVD [1]. Therefore, the need for continuous monitoring of BP in daily life is evident. In a clinical context, hypertension can be diagnosed when multiple readings of systolic BP (SBP) and diastolic BP (DBP) are above 140 and 90 mmHg, respectively [2]. Moreover, the BP pulse wave (PW_{BP}) presents a wealth of information on the cardiovascular system, providing remarkable insights for CVDs' diagnosis and prognosis at an early stage.

The gold standard for BP measurement is sphygmomanometry at the brachial artery, which besides being uncomfortable when used for long periods of time due to the periodic inflation and deflation of the cuff only provides discrete values of SBP and DBP. Contrarily, invasive BP measurement is continuous and accurate but attains a high risk as it comprises the insertion of a catheter in the artery of the patient and should only be used in an intensive care unit. The ideal BP sensor for continuous measurement should allow long-term monitoring, be noninvasive, and be easy to integrate with a remote healthcare system. There are several sensor-based techniques that try to answer the requirements listed above, such as the tonometer method, vascular unloading method, plethysmography (PPG), pulse transit time (PTT), and ultrasound (US)-based method [3], [4], [5]. Assessment of the BP waveform via the US technique utilizes a high-speed acoustic probe to capture the pulsation of arteries. On the one hand, echo signals and the Doppler shift principle have been used in this technique to detect arterial wall displacement and blood flow, which with a mathematical model and signal

Manuscript received 26 June 2022; accepted 11 October 2022. Date of publication 25 October 2022; date of current version 30 November 2022. This work was supported by B. Braun-Stiftung (NINUSSense) under Grant BBST-D-19-00008. The associate editor coordinating the review of this article and approving it for publication was Dr. Shanhong Xia. *(Thomas Stieglitz and Ana Belén Amado-Rey contributed equally to this work.) (Corresponding author: Ana Carolina Gonçalves Seabra.)*

Ana Carolina Gonçalves Seabra is with the Center for MicroElectroMechanical Systems (CMEMS-UMinho), University of Minho, 4710-057 Braga, Portugal, also with the Laboratory for Biomedical Microtechnology, Department of Microsystems Engineering, University of Freiburg, 79110 Freiburg, Germany, and also with the BrainLinks-BrainTools, Institute for Machine-Brain Interfacing Technology (IMBIT), University of Freiburg, 79110 Freiburg, Germany (e-mail: carolina.seabra@imtek.uni-freiburg.de).

Alexandre Ferreira da Silva is with the Center for MicroElectroMechanical Systems (CMEMS-UMinho), University of Minho, 4710-057 Braga, Portugal, and also with the LABBELS–Associate Laboratory, Braga, 4710-057 Guimarães, Portugal.

Thomas Stieglitz and Ana Belén Amado-Rey are with the Laboratory for Biomedical Microtechnology, Department of Microsystems Engineering, University of Freiburg, 79110 Freiburg, Germany, and also with the BrainLinks-BrainTools, Institute for Machine-Brain Interfacing Technology (IMBIT), University of Freiburg, 79110 Freiburg, Germany.

This article has supplementary downloadable material available at https://doi.org/10.1109/JSEN.2022.3215597, provided by the authors.

Digital Object Identifier 10.1109/JSEN.2022.3215597

1558-1748 © 2022 IEEE. Personal use is permitted, but republication/redistribution requires IEEE permission.
See https://www.ieee.org/publications/rights/index.html for more information.

Authorized licensed use limited to: UNIVERSITAET FREIBURG. Downloaded on March 10,2024 at 14:35:46 UTC from IEEE Xplore. Restrictions apply.

conditioning reveal good accuracy in arterial measurements and is, therefore, convenient to use. On the other hand, it is necessary to maintain stable contact between the probe and the measuring site to achieve a reliable acoustic coupling interface [3], [6], [7], [8], [9]. Taking the indicated advantages and disadvantages into account, the US-based method seems to be the most promising. Therefore, this article aims to provide research on the best BP model that can be applied to a US sensor for continuous and noninvasive measurement.

When using noninvasive methods of pressure measurement, various mathematical arterial models arise that relate a hemodynamic parameter to BP. The correlation of blood flow and/or artery distension with BP and different mathematical models that relate these arterial variables to the arterial PW_{BP} have been demonstrated [6], [7], [8], [9], [10]. The newest developed devices apply an exponential model to the artery's distending diameter. However, a direct comparison between the different mathematical models has never been done.

The goal is to develop a cuff-free wrist-worn device that examines hemodynamic changes in the radial artery and transforms them, according to the most precise BP model, into pulse pressure (PP) waveforms. By doing this, a continuous and accurate diagnosis can be provided. Up to now, noninvasive standard BP measurements are performed in the brachial artery with a cuff. Although DBP and mean arterial pressure (MAP) do not change significantly through the arterial tree [11], and the calibration of BP values taken from a different artery (i.e., brachial artery) than the artery under study (i.e., radial artery) is generally accepted, the methodology might lead to inaccurate readings and wrong clinical prognoses. Due to the effects of increased viscoelasticity, PP, defined as PP = SBP − DBP, changes through the arterial tree. Intraradial BP can present differences higher than 15 mmHg in comparison to the intrabrachial BP [12]. It is necessary to deduce an algorithm to continuously extract highly accurate SBP and DBP values from measurements in the radial artery.

This work performs an analytical analysis and comparative study between different mathematical arterial models based on their physical principles, with their assumptions and simplifications explained. A computer-simulated arterial pulse wave (PW) database developed by Charlton et al. [13] was used to demonstrate how the pressure values vary between different arteries and to compare the response to the models at different measuring sites. Due to the systemic arterial stiffening with age, the vascular profile and waveform change throughout one's life. As a fundamental study, this work focuses on young subjects between the ages of 25 and 35 years old, without age-induced arterial stiffness. In the in silico study, the accuracy of different mathematical models applied to the radial artery was investigated through parameters derived from the database. The models' error study was initially focused on PP since all models were calibrated to DBP at the brachial artery (DBP error is the same between models at each arterial site). The best-performing model was validated with a porcine artery and a customized US sensor. Data were postprocessed in a custom analysis program written in the MATLAB environment. Finally, the accuracy of the ex vivo measurements was studied through its comparison with a commercial sensor. The results showed promising advances and new insights for the extraction of vital parameters when using US sensors.

II. Pressure Waveform Models

For the application of a wrist-wearable device to measure BP through an US sensor, models that rely on the measurement of the hemodynamics of the arterial segment were analyzed.

A. Model 1 (M1): Linear Relationship

Through a direct conversion, the diameter waveform, $D(t)$, can be projected to a pressure waveform [6]. The end-diastolic and mean arterial diameter, D_d and $\bar{D}(t)$, respectively, are calibrated to the brachial DBP and MAP, deriving the following conversion factor k:

$$k = \frac{\text{MAP} - \text{DBP}}{\bar{D}(t) - D_d}. \tag{1}$$

The diameter waveform is then converted to the pressure waveform by the factor k (1) and the slope-intercept b is calculated at the diastolic pressure

$$P(t) = D(t) \cdot k + b. \tag{2}$$

Although a study revealed that this method of assessing BP may on average only underestimate invasive PP by 1.6 mmHg [14], this is not expected if the measurement is taken in the periphery. In normotensive subjects, the diameter of elastic arteries (e.g., carotid artery) changes linearly with pressure, while peripheral arteries (e.g., radial artery) exhibit saturation at near-systolic pressure [15]. In vitro and in vivo studies have demonstrated that the diameter–pressure relationship exhibits an exponential characteristic [6], [15], [16].

B. Model 2 (M2): Exponential Relationship

Many researchers have studied the exponential relationship between arterial diameter distension and BP [6], [8], [10], [17]. After obtaining the arterial vessel cross-sectional area, $A(t)$, from $D(t)$, the BP waveform can be calculated as follows:

$$P(t) = P_0 \cdot e^{\alpha\left(\frac{A(t)}{A_d} - 1\right)} \tag{3}$$

with

$$\alpha = \frac{A_d \cdot \ln(P_s/P_d)}{A_s - A_d} \tag{4}$$

where α is the vessel rigidity coefficient, P_0 and P_d are the diastolic pressures, P_s is the diastolic pressure, A_d is the diastolic luminal area, and A_s the systolic luminal area.

As (3) is valid over a large pressure range [6], α is pressure-independent and constant. To accurately determine α, it is worth noting that P_s and P_d must be obtained at the same position as $D(t)$. If the pressures are unknown, calibration of the brachial sphygmomanometer could be done. Wang et al. [8] designed an ultrasonic device that uses the brachial calibration method with a measurement precision higher than 2 mmHg. However, it is known that P_s changes drastically through the arterial tree and it should not be used for calibration in other measuring sites, especially if the changes between SBP are known to be very different as is the case between the brachial and radial artery [12].

In addition, an iterative correction of α was proposed by Meinders and Hoeks [6]. For the first iteration, the rigidity coefficient, α_i with $i = 1$, is calculated as indicated in (4), taking use of brachial SBP as P_s. After determining $P_i(t)$, the

Authorized licensed use limited to: UNIVERSITAET FREIBURG. Downloaded on March 10,2024 at 14:35:46 UTC from IEEE Xplore. Restrictions apply.

measured mean pressure $\bar{P}_i(t)$ is compared to the MAP determined at the brachial artery. If $|\bar{P}_i(t) - \text{MAP}| > 0.01$ mmHg, a new α_{i+1} is calculated until the mean pressure of the projected waveform converges to brachial MAP. The iterative α_{i+1} is calculated as follows:

$$\alpha_{i+1} = \alpha_i \cdot \frac{\text{MAP}}{\bar{P}_i(t)}. \tag{5}$$

C. Model 3 (M3): Laplace's Law + MK

An US-based method for the assessment of PW_{BP} based on the integration of pressure was introduced by Vappou et al. [7]. The method relies on the measurement of local distension waveforms using US signals, together with the measurement of the local PW velocity (PWV) that leads to an estimation of the local stiffness. The theoretical principle combines Laplace's Law and the Moens–Korteweg (MK) equation.

Laplace's law

$$dP = \frac{E \cdot h \cdot dR}{R^2} \tag{6}$$

relates an infinitesimal variation of the lumen radius dR to the variation of internal fluid pressure dP, where E is Young's elastic modulus of the arterial wall, h is the wall thickness, and R is the artery's luminal radius.

The MK equation relates the PWV to the elasticity of the arterial wall

$$\text{PWV} = \sqrt{\frac{E \cdot h}{2\rho \cdot R}} \tag{7}$$

where ρ is the blood density.

By replacing the elasticity factor in (6) with E calculated from (7), and integrating it over the cardiac cycle, the PP waveform is given by

$$\Delta P = 2\rho \cdot \text{PWV}^2 \cdot \log\left(\frac{R(t)}{R_0}\right) \tag{8}$$

with $\Delta P = P(t) - P_0$, and P_0 and R_0 corresponding to diastolic values of pressure and artery radius, respectively. As in the most indirect BP measurement models, the methodology of Vappou et al. [7] only determines ΔP, maintaining P_0 unknown. A conversion to absolute BP measurement is done by adding DBP measured at the brachial artery to ΔP calculated in (8).

In this study, a linear waveform calibration to brachial DBP and MAP was proposed. The calibration procedure takes the model's projected mean pressure $\bar{P}(t)$ (through integration over a cardiac cycle) and end-diastolic pressure P_{end} to calculate the calibrating factor m as

$$m = \frac{\text{MAP} - \text{DBP}}{\bar{P}(t) - P_{\text{end}}}. \tag{9}$$

The pressure waveform is then multiplied by the calibration factor and the slope-intercept b is added (calculated for $P(t) = \text{MAP}$).

In the study with 11 subjects [7], a good correlation ($0.94 < r < 0.98$) was found between PP measured through radial tonometry using a commercially available system and PP obtained through the method described above. The Bland–Altman study [7] revealed a positive bias of 4.7 mmHg and a standard deviation (SD) of 4.45 mmHg.

D. Model 4 (M4): Bramwell–Hill Equation

Bramwell and Hill [18] improved the MK equation such that the formula may be independent of Young's modulus E and thickness h of the vessel wall, directly relating PWV to the compliance dA/dP as follows:

$$\text{PWV} = \sqrt{\frac{A(t) \cdot dP}{\rho \cdot dA}}. \tag{10}$$

By rearranging (10), and assuming that PWV remains relatively constant during a cardiac cycle, a pressure waveform can be expressed in terms of PWV and change in cross-sectional area as [19]

$$P(t) - P_0 = \rho \cdot \text{PWV}^2 \cdot \ln\left(\frac{A(t)}{A_0}\right). \tag{11}$$

It should be noted that the PWV is dependent on the compliance and area of an artery and it should be determined at the local site of diameter distension measurement [19].

The same calibration procedure as in M3 was applied to this model.

E. Model 5 (M5): Joukowsky's Equation + PWV

Soleimani et al. [9] developed a system where the internal diameter and blood velocity waveforms were extracted from consecutive sonograms. The authors assume that blood is an incompressible fluid traveling through a flexible tube, and pressure can be determined through the fundamental water hammer phenomenon. Thus, the water hammer principle can be projected to the arterial vascular system, where the opening and closing of cardiac valves correspond to mechanical valves in a hydraulic piping system. The water hammer equation, known as Joukowsky's equation, measures the change in pressure of a fluid resulting from a change in the fluid's velocity, taking into account its density and PWV

$$\Delta P = \rho \cdot \text{PWV} \cdot \Delta v \tag{12}$$

where ΔP and Δv are changes in pressure and velocity, respectively, relative to the initial value.

Solving (12) with (10), and applying the increment of pressure and area instead of its derivative, results in

$$\Delta P = \rho \cdot (\Delta v)^2 \cdot \frac{A(t)}{\Delta A} \tag{13}$$

where, once again, relative ΔP is obtained instead of the absolute BP. The brachial DBP is then added to the measured pressure and the absolute PW_{BP} is determined. Soleimani et al. [9] developed a subject-specific calibration procedure based on the correlation between $\bar{P}(t)$ calculated from the proposed model and $\bar{P}(t)$ calculated from tonometry measurements at the radial artery. The calibrated model was validated on 20 male subjects via a standard sphygmomanometer, revealing a PP correlation of 0.91 and mean absolute difference (through Bland–Altman analysis) of (1.333 ± 6.548) mmHg [9].

F. Comparison Between Models

It is worth noting the similarities between models M3 and M4. Both (8) and (11) are derived from the Bramwell–Hill

Authorized licensed use limited to: UNIVERSITAET FREIBURG. Downloaded on March 10,2024 at 14:35:46 UTC from IEEE Xplore. Restrictions apply.

TABLE I
MODEL EQUATIONS AND CALIBRATION PROCEDURE

	Name	Equation	Calibration	Reference
M1	Linear Relationship	$P(t) = D(t) \cdot k + b$	$k = \frac{MAP - DBP}{\bar{D}(t) - D_d}$	[6]
M2	Exponential Relationship	$P(t) = P_0 \cdot e^{\alpha(\frac{A(t)}{A_d} - 1)}$	α_1 with $P_s = SPB$ and $P_d = DBP$; $\alpha_{i+1} = \alpha_i \cdot \frac{MAP}{\bar{P}_i(t)}$	[6]
M3	Laplace's Law + MK equation	$P(t) - P_0 = 2\rho \cdot PWV^2 \cdot log(\frac{R(t)}{R_0})$	$P(t)$ calibrated to $m = \frac{MAP - DBP}{\bar{P}(t) - P_{end}}$	[7]
M4	Bramwell-Hill Equation	$P(t) - P_0 = \rho \cdot PWV^2 \cdot ln(\frac{A(t)}{A_0})$		[19]
M5	Joukowsky's Equation + PWV	$P(t) - P_0 = \rho \cdot (\Delta v)^2 \cdot \frac{A(t)}{\Delta A}$	correlation between M5 $\bar{P}(t)$ and $\bar{P}(t)$ from tonometry measurements at the radial artery	[9]

P_0 calibrated to DBP. DBP, SBP and MAP calculated from brachial sphygmomanometer.

equation that relates the MK equation to Laplace's Law. However, when integrating over a cardiac cycle, Vappou et al. [7] proposed a model with the decimal logarithm, while the direct integration of the Bramwell–Hill equation applies the natural logarithm. Although it is expected that both models produce similar responses, the raw, noncalibrated BP values derived from (11) are higher than the ones obtained from (8). This changes after applying the corresponding MAP and DBP calibration, where both calibrated models exhibit the same curve. From here on, M3/4 refers to both calibrated models M3 and M4.

Table I summarizes the different model equations and the implemented calibration methods. All models are calibrated with DBP and MAP. In M2, the first iteration is calibrated with SBP. Calibrating values DBP, SBP, and MAP can be taken from a brachial sphygmomanometer measurement.

III. MATERIALS AND METHODS

A. Database

For the benchmarking of the different PW_{BP} models, the *open-source* simulated database of arterial PWs developed by Charlton et al. [13] was used. The computational model consists of three main components, based on the work of Alastruey et al. [20]. First, the arterial tree is decomposed into arterial segments modeled as thin viscoelastic tubes of constant length and linearly tapered diameter. Then, a periodic inflow waveform is introduced at the aortic root. Third, terminal three-element Windkessel boundary conditions are imposed at the outlets of peripheral arterial segments, modeling vascular beds. The database was validated by the comparison of PWs and hemodynamic characteristics with in vivo data.

The primary parameters (flow velocity and luminal area) that can be directly extracted from US measurements were taken from the database and then simulated in MATLAB for a comparative realistic analysis of the different five models. Fig. 1 shows the compliance curves derived from the baseline of a 25-year-old virtual subject (one simulated subject created with the age-specific mean values for all variables, e.g., heart rate, stroke volume, and arterial diameters). As seen in Fig. 1, it is clear that there is a change in behavior and compliance through the arterial tree, so that the carotid artery presents an approximately linear relationship, while toward the periphery, in the radial artery, the hysteresis is much more accentuated due to the collagen content. Thus, when performing arterial parameters readings with the US in the arterial tree (i.e., BP measurements), changes through the different arteries are expected. Therefore, specific models or concrete stiffness coefficients should be applied to each local peripheral artery in the cardiovascular tree.

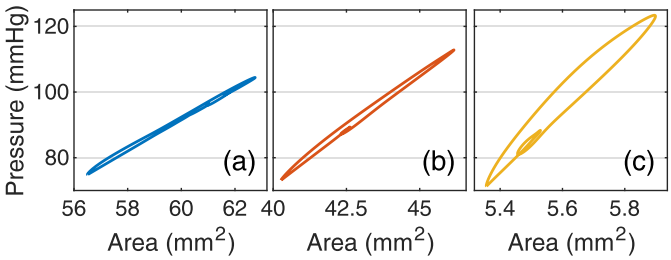

Fig. 1. Compliance curves (P/A) for (a) carotid, (b) brachial, and (c) radial artery, extracted from the Charlton database [13] (for the baseline subject). The increase in hysteresis and PP toward the periphery due to an increase in stiffness is noticeable.

B. Models Simulation

To evaluate and analyze the changes in the hemodynamic parameters in the arterial tree, the five BP models were studied at three main arteries: carotid, brachial, and radial. For each measuring sites, luminal area PW, in combination with: 1) PWV for M3 and M4 and 2) flow velocity PW for M5, were extracted from the database and applied to each model. As DBP and MAP do not change significantly through the arterial tree [11], calibration was made to brachial DBP and MAP (additionally to SBP in the case of M2). The aim of calibrating the curves to the brachial values is to approximate the simulation to a practical situation where calibration of the measured hemodynamic PWs and values would be done using a brachial sphygmomanometer. Furthermore, to maintain real-life application plausibility, brachial MAP was not calibrated to its gold standard integration of BP curve over a cardiac cycle but through a mathematical equation that can be derived from brachial-cuff measurements. This correlates SBP and DBP to MAP. Hence, brachial MAP was calculated as $MAP = 0.42 \cdot SBP + 0.58 \cdot DBP$ [21].

The process explained above was applied to the 1458 simulated young subjects (between 25 and 35 years old) available in the database. Next, the resulting PP models were compared and correlated with the *ground-truth* PP waveforms (PW_{PP}) supplied by the database ($PW_{PP} = PW_{BP} - DBP$). Additionally, error boxplots for DBP, MAP, SBP, PP, and mean PW_{BP} with its SD were calculated and compared to the *ground-truth* values (from the database).

C. Ex Vivo Validation

To determine the validity of the study, measurements with the most accurate model were performed in an ex vivo setup

Authorized licensed use limited to: UNIVERSITAET FREIBURG. Downloaded on March 10,2024 at 14:35:46 UTC from IEEE Xplore. Restrictions apply.

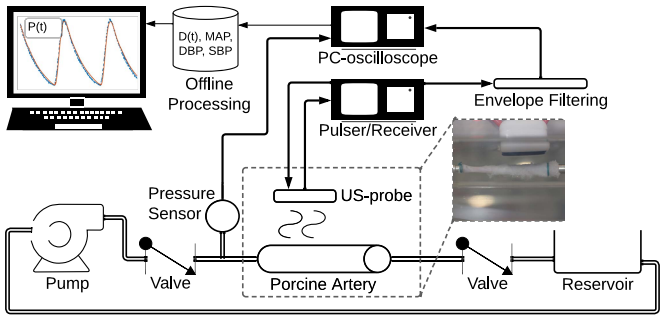

Fig. 2. Diagram of the setup for ex vivo BP model validation. Double lines represent the fluid path, thick arrows the analog signal, and thin arrows the digital signal.

(see Fig. 2). The mimicked arm consisted of a porcine artery (inlet diameter = (4.09 ± 0.59397) mm, outlet diameter = (4.095 ± 1.4637) mm) submerged in saline solution (%w/w = 0.9%) to prolong the artery's viability by maintaining a similar physiological osmotic pressure. The pulsatile flow was established by a "heart-like" pump (Zentrifugalpumpe MultiFlow, GAMPT GmbH, Germany), which regulates the flow to a negative sawtooth configuration, and mimics the heart waveform, with a rapid increase in pressure (systole) followed by a slow decrease (diastole). Two nonreturn valves at the inlet and outlet of the artery controlled the flow.

The distending diameter of the artery was measured through a custom ultrasonic echo-wall tracking algorithm previously validated [22]. The custom-made 5-MHz resonance-frequency US-probe (Fraunhofer IBMT, Germany) was driven by a general-purpose ultrasonic pulser/receiver (DPR300 Pulser/Receiver, Imaginant Inc., NY) with a pulse frequency rate of 2 kHz. The acting piezoelectric element (made of lead zirconate titanate (PZT) with a dimension of 10×5 mm^2) functions both as sender and receiver (Tx/Rx) of the acoustic signal, granting a perpendicular reading of the vessel wall echoes. For easier postprocessing, the raw analog echo signal was filtered and the signal envelope of the received echoes was recorded through a new low-power peak detector [22]. The signal envelope captured by the US, along with the pressure signals from the Honeywell Sensor, was acquired by a PC-oscilloscope (Picoscope 5243D, Pico Technology Ltd., U.K.) at a sampling frequency of 500 MHz, an ADC resolution of 8 bits, and post-processed offline in MATLAB.

The derived pressure was compared to the pressure measured by a commercial pressure sensor (ABP Series, Honeywell International Inc.). The flow rate was varied between 3000 and 4000 r/min to introduce different pressure ranges similar to the in silico study (mean PP of (52.644 ± 10.502) mmHg). After extracting each full cardiac cycle from the ex vivo trial, in resemblance to the in silico study analysis, the PP mean difference and linear correlation were calculated, followed by determining the mean PW and SBP error.

IV. Results

A. Models Simulation

The BP curves were derived by applying the five pressure models to the PWs from the 25-year-old baseline subject (see Fig. 3). Note that after calibration, M3 and M4 exhibit the same waveform, and thus only one curve is shown in the graph. Overestimation of SBP (and consequently, PP) was seen in M2 and M5. Except for M5, all PWs models were in good agreement with the pressure waveform except for a slight time delay. The waveform profile for M5 is not in accordance with the rest of the models, as it is modeled from the blood flow velocity profile, and not only from the arterial distension waveform. Due to the calibration procedure being done with brachial DBP, underestimation and overestimation of DBP are seen at the carotid artery and radial artery, respectively. An increase in the time delay between *ground truth* and the model's waveform is seen toward the periphery.

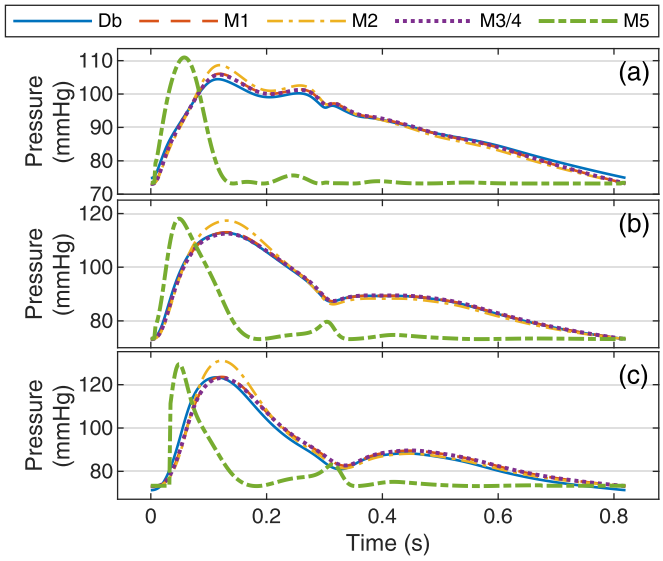

Fig. 3. BP models performance for the 25-year-old baseline subject at (a) carotid, (b) brachial, and (c) radial artery. All models are calibrated as described in Section II. Notice that M1 and M3/M4 curves overlap. Curve Db refers to the database pressure waveform (*ground truth*).

Pearson's linear correlation r and mean difference PPs obtained from the models were compared based on PPs extracted from the database (Table II, for correlation and Bland–Altman plots, see Supplementary note A). The study was done with the database's young subjects ($n = 1458$) at the carotid, brachial, and radial artery. There is a remarkable improvement of the calibrated models in comparison to uncalibrated (M*X*') ones, noticeable by the high increment of r. Notice that only uncalibrated M3', M4', and M5' were introduced, as M1 and M2 calibration procedure is intrinsic to the model. In all the measuring sites, M5 is always the least accurate, followed by M2. At the carotid artery, M3/4 exhibit slightly better performance in r and mean difference, while at the brachial and radial artery, the r is the same between models M1 and M3/4. Moreover, when comparing M1 and M3/4 at the radial artery, it is appreciated that for M1 the mean difference is slightly lower than M3/4. In summary, M1 is the best-performing model in the radial artery, revealing a correlation of 0.978 and a mean difference of (-2.845 ± 2.565) mmHg.

After rejecting M5 because of its high error variability (±9.215 mmHg) and low correlation (0.500) with the PP extracted from the database, further error studies between the best performing models were done. DBP and MAP display

Authorized licensed use limited to: UNIVERSITAET FREIBURG. Downloaded on March 10,2024 at 14:35:46 UTC from IEEE Xplore. Restrictions apply.

TABLE II
PEARSON'S LINEAR CORRELATION AND MEAN DIFFERENCE BETWEEN PP MODELS AND SBP ERROR FOR THE BEST MODELS (M1, M2, M3/4). STUDIES ($n = 1458$) AT THE CAROTID, BRACHIAL, AND RADIAL ARTERY

	Carotid artery		Brachial artery		Radial artery	
	r-Pearson	Mean difference (mmHg)	r-Pearson	Mean difference (mmHg)	r-Pearson	Mean difference (mmHg)
M1	0.979	2.899 ± 1.799 SBP: 0.895 ± 1.719	**0.988**	**-0.566 ± 1.984** SBP **-0.566 ± 1.985**	**0.978**	**-2.845 ± 2.565** SBP: **-0.761 ± 2.213**
M2	0.969	5.554 ± 2.007 SBP: 3.549 ± 1.829	0.983	3.857 ± 1.730 SBP: 3.856 ± 1.731	0.969	4.549 ± 2.936 SBP: 6.632 ± 2.707
M3'	0.422	-19.065 ± 7.312	0.324	-25.295 ± 8.796	0.711	-31.762 ± 8.254
M4'	0.422	-4.036 ± 7.681	0.324	-5.195 ± 9.823	0.711	-4.561 ± 7.485
M3/4	**0.980**	**2.640 ± 1.792** SBP: **0.635 ± 1.727**	**0.988**	-1.031 ± 2.044 SBP: -1.031 ± 2.045	**0.978**	-3.328 ± 2.641 SBP: -1.244 ± 2.289
M5'	0.882	-12.981 ± 4.382	0.774	-16.038 ± 6.021	0.506	-15.981 ± 9.161
M5	0.881	7.026 ± 4.393	0.773	4.047 ± 6.028	0.500	4.236 ± 9.215

MX' identifies uncalibrated model.

the same error profile between the remaining models (see Supplementary note B), since the models are calibrated from the brachial DBP and MAP (the error was null at the brachial artery). As expected, an overestimation of DBP was measured at the carotid artery, with an error of (-2.004 ± 0.782) mmHg, and an underestimation of DBP at the radial artery, with an error of (2.084 ± 0.639) mmHg.

The results of the error studies are depicted in the boxplots in Fig. 4, where mean PW error, its SD and SBP error are included (additionally, the SBP mean error values are shown in Table II for the best models). Even though M2 always exhibits a lower mean PW error at the carotid artery (c.a. $= -0.590$ mmHg) and at the radial artery (r.a. $= 0.999$ mmHg), the SD (i.e., r.a. $= 2.748$ mmHg) and SBP error (i.e., r.a. $= 6.632$ mmHg) are higher in all arterial sites. The mean PW error is the same in M1 and M3/4 at all sites (i.e., r.a. $= 1.007$ mmHg). In the carotid artery, M3/4 has a smaller SD and SBP error (0.918 and 0.635 mmHg, respectively) than M1 (0.975 and 0.895 mmHg, respectively). However, at the brachial artery (b.a.) and radial artery M1 has a lower SD (b.a. $= 0.721$ mmHg, r.a. $= 2.122$ mmHg) and SBP error (b.a. $= -0.566$ mmHg, r.a. $= -0.761$ mmHg) than M3/4 (i.e., SBP error: b.a. $= 0.768$ mmHg, r.a. $= -1.244$ mmHg). Thus, it is corroborated that in a 1458 subject study, M1 is the most accurate model for the radial artery.

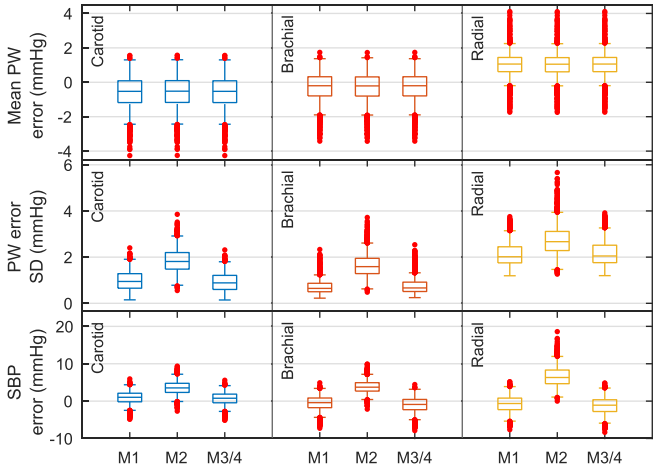

Fig. 4. BP models error ($n = 1458$) at the carotid, brachial, and radial artery for the best models (M1, M2, M3/4). The first and second rows illustrate the mean PW error and its SD. SBP error is shown in the third row.

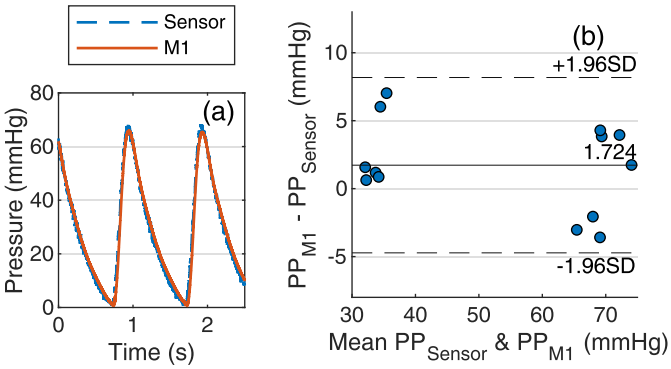

Fig. 5. Comparison between the commercial pressure sensor and the linear model (M1). (a) Pressure waveforms of an exemplary trial. (b) Bland–Altman plot for the ex vivo PP study ($n = 13$).

B. Ex Vivo Validation

Once the linear model (M1) was selected as the best-performing model, it was validated ex vivo. In total, 13 full cardiac-like cycles were extracted from the ex vivo study and analyzed. The pressure sensor measured a mean PP of (52.168 ± 19.276) mmHg. Fig. 5(a) shows the pressure waveforms (pressure measured by the sensor and pressure derived by the linear model) for one exemplary trial. The PP mean difference was (1.724 ± 3.291) mmHg, the Bland–Altman plot is shown in Fig. 5(b), and PP Pearson's linear correlation was $r = 0.988$. A mean PW difference of (3.156 ± 6.654) mmHg, DBP error of (0.831 ± 0.388) mmHg, and SBP error of (2.555 ± 3.232) mmHg were calculated between the linear model and pressure sensor.

V. DISCUSSION

US-based methods are feasible in most vascular sites and cost-effective, being promising as indirect, noninvasively, continuous, and comfortable means of obtaining arterial pressure waveforms, and providing anatomical and functional information about arterial health. Several models have been proposed that relate hemodynamic variables indirectly to BP. In the present work, five models that ultimately take the distending luminal area were studied in silico through an arterial PW simulated database. To the best of our knowledge, this was the first time a comparison study of BP models was done in a large ($n = 1458$) and variable database.

Authorized licensed use limited to: UNIVERSITAET FREIBURG. Downloaded on March 10,2024 at 14:35:46 UTC from IEEE Xplore. Restrictions apply.

All the studied models rely on the physical assumptions that the luminal area is a circle, neglecting the possibility of the irregular and asymmetric area and, therefore, excluding the cases of highly torturous arteries. Additionally, the models assume linear elasticity, meaning that pressure and luminal area PWs have the same temporal profile. However, due to the natural viscoelasticity of arteries, this is known not to be true and it is corroborated in this study with the compliance curves and the time delay between the *ground-truth* pressure and the calculated PW_{BP} from the different models. The time delay is larger at the radial artery, due to the increase in collagen content and, consequently, viscoelasticity.

Another common limitation between the models is that all noninvasively acquired arterial pressure waveforms require calibration to a known BP, imposing potential sources of measurement errors. It is generally accepted that DBP and MAP do not change considerably through the arterial tree, however, there are small changes, as seen in this study, introducing over- and underestimation in DBP at the carotid and radial artery, respectively, when calibrated to brachial DBP. Furthermore, every formula to calculate MAP that uses a form factor (FF) that quantifies the change in the shape of PW_{BP} and relates its mean pressure to SBP and DBP is known to have flaws. As the shape of BP changes along the artery tree due to propagation and reflection phenomena, it is understandable that a common MAP equation is not possible. A study by Papaionnou et al. [21] demonstrated that the estimation of MAP using the FF value 0.412 provide results that are more accurate to invasive brachial MAP calculation when compared with MAP determined by the traditional formula, which uses $FF = 0.3$. In the current work, $FF = 0.412$ was used to best approximate brachial MAP to its true value.

All models except for M5 were able to approximate the shape of their BP waveform to the *ground truth*. The differences between the shapes can be appointed to M5 taking the flow velocity profile into account, while for the rest of the models the only time-dependent variable is the change in the luminal area and its shape is similar to the pressure PW. The M5 pressure shape shown in Fig. 3 converges with the one displayed by Soleimani et al. [9], which is characterized by a distinct and separate two-peak waveform. Nonetheless, it should be noted this model is able to extract the hemodynamic properties (DBP, SBP, and PP) which deems it reasonable to be included in the present state-of-the-art pressure model study. Additionally, it is worth noting that the calibration procedure proposed by the authors could not be applied in the current study and was instead performed with the values available in the article [9]. This underlying impracticability may be the subject of an increased PW_{BP} error.

The simulation study showed a slight difference in the best applicable model at different measuring sites. However, while theoretically, the carotid artery exhibits a more linear compliance behavior than the radial artery, M3/4 (logarithmic model) proved to have a lower error value than M1 (linear model). The contrary was seen at the radial artery, where although there is a stronger viscoeleasticity and arterial rigidity, M1 turned out to be the model with the lowest error. Nonetheless, the differences in error between M1 and M3/4 are quite small ($<$0.5 mmHg) and may be neglected.

The Association for the Advancement of Medical Instrumentation (AAMI) recommends a maximum mean difference of ± 5 mmHg and SD of ± 8 mmHg between the standard and the novel method of pressure measurement (AAMI/ISO 81060–2:2013) [23]. Taking the database's PW_{BP} as standard, M1 and M3/4 accomplished this requirement in all hemodynamic properties and arterial sites, while M2 and M5 did not comply with the recommendations at the carotid and radial artery (e.g., M2 had an SBP error of (7.602 ± 2.622) mmHg at the radial artery). As the exponential relationship is the most used model for extracting pressure waveform from US measurements of arterial wall distensibility in known literature review [6], [8], [10], it was expected that M2 would reveal a better accuracy than M1 (linear model) but that was not the case. While the linear model (M1) follows AAMI recommendations and has the best results in the brachial and radial artery, the exponential model (M2) metrics are above the recommended values and are the second worst-performing model in the current study.

The best-performing model was studied ex vivo in similar PP ranges as in the in silico study (see Supplementary note C for PP range comparison), providing an adequate validation. The ex vivo study revealed a better correlation ($r = 0.988$) than in silico ($r = 0.978$). This may be due to the fact that the model's calibration in ex vivo was done by using the in-site pressure sensor's DBP and MAP recording. Thus, the calibration was done specifically to the measured artery (radial) and not to the brachial artery, which increases the error for comparison with realistic and practical measurements.

It is commonly known that an individual's vascular, and therefore, hemodynamic properties change with age. It would be expected that the best-performing model is different for elderly populations, possibly according to the stiffness of the artery. However, this discussion is beyond the scope of this study. By focusing on young subjects (25 and 35 years old), the authors have brought up novel methodologies and findings on BP pressure models to the scientific community and hope to instigate further research.

VI. Conclusion

The present study provides a novel in silico analytical comparison between different models that relate arterial PWs to the pressure waveform for continuous, noninvasive monitoring of arterial health parameters. The best model for the radial artery has been validated with an ex vivo experiment, in which a porcine artery and an US sensor were used. The ex vivo experimental measurements demonstrated the high accuracy of the linear model based on the MAP calibration with low error values of (1.724 ± 3.291) mmHg. This research introduces a new insight into the extraction of arterial parameters based on the US that will help the researchers to get much more precise clinical noninvasive readings. The changes in the pressure waveform through the arterial tree and age-induced arterial stiffening make it necessary for a site-specific and vascular age-specific model calibration method for a highly accurate noninvasive sensor measurement.

Acknowledgment

The authors would like to thank Fraunhofer-Institut für Biomedizinische Technik (IBMT), Sulzbach, Germany, for providing the US sensor.

Authorized licensed use limited to: UNIVERSITAET FREIBURG. Downloaded on March 10,2024 at 14:35:46 UTC from IEEE Xplore. Restrictions apply.

REFERENCES

[1] (2019). *Hypertension*. World Health Organization. [Online]. Available: https://www.who.int/news-room/fact-sheets/detail/hypertension

[2] T. Unger et al., "2020 international society of hypertension global hypertension practice guidelines," *Hypertension*, vol. 75, no. 6, pp. 1334–1357, Jun. 2020.

[3] R. Mukherjee, S. Ghosh, B. Gupta, and T. Chakravarty, "A literature review on current and proposed technologies of noninvasive blood pressure measurement," *Telemedicine e-Health*, vol. 24, no. 3, pp. 185–193, Mar. 2018.

[4] T. Arakawa, "Recent research and developing trends of wearable sensors for detecting blood pressure," *Sensors*, vol. 18, no. 9, p. 2772, Aug. 2018.

[5] C. Peng, M. Chen, H. K. Sim, Y. Zhu, and X. Jiang, "Noninvasive and nonocclusive blood pressure monitoring via a flexible piezo-composite ultrasonic sensor," *IEEE Sensors J.*, vol. 21, no. 3, pp. 2642–2650, Feb. 2021.

[6] J. M. Meinders and A. P. G. Hoeks, "Simultaneous assessment of diameter and pressure waveforms in the carotid artery," *Ultrasound Med. Biol.*, vol. 30, no. 2, pp. 147–154, 2004.

[7] J. Vappou, J. Luo, K. Okajima, M. di Tullio, and E. Konofagou, "Pulse wave ultrasound manometry (PWUM): Measuring central blood pressure non-invasively," in *Proc. IEEE Int. Ultrason. Symp.*, Oct. 2011, pp. 2122–2125.

[8] C. Wang et al., "Monitoring of the central blood pressure waveform via a conformal ultrasonic device," *Nature Biomed. Eng.*, vol. 2, no. 9, pp. 687–695, Sep. 2018.

[9] E. Soleimani, M. Mokhtari-Dizaji, N. Fatouraee, and H. Saberi, "Assessing the blood pressure waveform of the carotid artery using an ultrasound image processing method," *Ultrasonography*, vol. 36, no. 2, pp. 144–152, Apr. 2017.

[10] B. Gavish and J. L. Izzo, "Arterial stiffness: Going a step beyond," *Amer. J. Hypertension*, vol. 29, no. 11, pp. 1223–1233, Jul. 2016.

[11] A. L. Pauca, M. F. O'rourke, and N. D. Kon, "Prospective evaluation of a method for estimating ascending aortic pressure from the radial artery pressure waveform," *Hypertension*, vol. 38, no. 4, pp. 932–937, 2001.

[12] M. K. Armstrong et al., "Brachial and radial systolic blood pressure are not the same," *Hypertension*, vol. 73, no. 5, pp. 1036–1041, May 2019.

[13] P. H. Charlton, J. Mariscal Harana, S. Vennin, Y. Li, P. Chowienczyk, and J. Alastruey, "Modeling arterial pulse waves in healthy aging: A database for in silico evaluation of hemodynamics and pulse wave indexes," *Amer. J. Physiol.-Heart Circulatory Physiol.*, vol. 317, no. 5, pp. H1062–H1085, Nov. 2019.

[14] L. M. V. Bortel et al., "Non-invasive assessment of local arterial pulse pressure: Comparison of applanation tonometry and echo-tracking," *J. Hypertension*, vol. 19, no. 6, pp. 1037–1044, Jun. 2001.

[15] A. P. G. Hoeks, "Non-invasive study of the local mechanical arterial characteristics in humans," in *Developments in Cardiovascular Medicine*. Amsterdam, The Netherlands: Springer, 1993, pp. 119–134.

[16] C.-K. Sun, "Cardio-ankle vascular index (CAVI) as an indicator of arterial stiffness," *Integr. Blood Press Control*, vol. 6, pp. 27–38, 2013.

[17] M. Kachuee, M. M. Kiani, H. Mohammadzade, and M. Shabany, "Cuffless blood pressure estimation algorithms for continuous health-care monitoring," *IEEE Trans. Biomed. Eng.*, vol. 64, no. 4, pp. 859–869, Apr. 2017.

[18] J. C. Bramwell and A. V. Hill, "The velocity of pulse wave in man," *Proc. Roy. Soc. London B, Biol. Sci.*, vol. 93, no. 652, pp. 298–306, Apr. 1922.

[19] J. Seo, S. J. Pietrangelo, H.-S. Lee, and C. G. Sodini, "Noninvasive arterial blood pressure waveform monitoring using two- element ultrasound system," *IEEE Trans. Ultrason., Ferroelectr., Freq. Control*, vol. 62, no. 4, pp. 776–784, Apr. 2015.

[20] J. Alastruey, K. Parker, and S. Sherwin, "Arterial pulse wave haemodynamics," in *Proc. 11th Int. Conferences Pressure Surges*, Dec. 2012, pp. 401–442.

[21] T. G. Papaioannou et al., "Mean arterial pressure values calculated using seven different methods and their associations with target organ deterioration in a single-center study of 1878 individuals," *Hypertens Res.*, vol. 39, no. 9, pp. 640–647, May 2016.

[22] A. B. Amado-Rey, A. C. G. Seabra, F. J. Becker, M. Fournelle, and T. Stieglitz, "Extraction of radial-artery strain and stiffness by using noninvasive ultrasound and a low-power peak detector," *IEEE Sensors Lett.*, vol. 5, no. 8, pp. 1–4, Aug. 2021.

[23] A. N. S. Institute, *Non-Invasive Sphygmomanometers—Part 2: Clinical Investigation of Automated Measurement Type*, Standard ANSI/AAMI/ISO 81060-2:2013, 2013. [Online]. Available: http://webstore.ansi.org

Ana Carolina Gonçalves Seabra received the B.S. degree in biomedical engineering and the M.Sc. degree in medical electronics from the University of Minho (UMinho), Braga, Portugal, in 2019 and 2021, respectively. She is currently pursuing the Ph.D. degree with the Laboratory of Biomedical Microtechnology (BMT), University of Freiburg, Freiburg, Germany. Her master's thesis was developed in collaboration with BMT, University of Freiburg, where she worked on blood pressure measurement research.

Alexandre Ferreira da Silva received the M.Sc. degree in biomedical engineering and the Ph.D. degree in leaders for technical industries from the University of Minho (UMinho), Braga, Portugal, in 2007 and 2011, respectively.

From 2011 to 2021, he was an Invited Assistant Professor with UMinho. From 2018 to 2021, he was an Executive Coordinator of the MIT Portugal Program. He is currently an Assistant Professor with the Department of Industrial Electronics, UMinho.

Thomas Stieglitz (Fellow, IEEE) received the Diploma degree in electrical engineering from Technische Hochschule Karlsruhe (now KIT), Karlsruhe, Germany, in 1993, and the Ph.D. and Habilitation degrees from Saarland University, Saarbrücken, Germany, in 1998 and 2002, respectively.

Since 2004, he has been a Full Professor of Biomedical Microtechnology with the Department of Microsystems Engineering, University of Freiburg, Freiburg, Germany. His research interests include neural implants and the monitoring of biological signals.

Ana Belén Amado-Rey received the Dipl.-Ing. and master's degrees in telecommunication engineering from the University of Extremadura, Cáceres, Spain, in 2010 and 2014, respectively, and the Ph.D. degree from the University of Freiburg, Freiburg, Germany, in 2018.

From 2014 to 2018, she was with Fraunhofer IAF, Freiburg, where she was involved with GaAs mHEMT technology. After her Ph.D. degree, she joined the Laboratory of Biomedical Microtechnology (BMT), University of Freiburg, Freiburg. Her main research interests include PCB electronic development at ultrasound (US) frequencies and piezo-characterization.

Authorized licensed use limited to: UNIVERSITAET FREIBURG. Downloaded on March 10,2024 at 14:35:46 UTC from IEEE Xplore. Restrictions apply.